Showcasing collaborative research from Professor Nakanishi's laboratory at National Institute for Materials Science (NIMS), Warsaw University of Technology, Tokyo Institute of Technology, and Shinshu University.

Supercooling of functional alkyl-π molecular liquids

The issue of occurrence of unexpected supercooling in alkylated-π functional molecular liquids (FMLs) was carefully investigated and a method of quickly identifying which FMLs are susceptible to supercooling was designed. Finally, in order to prevent supercooling a rational molecular design strategy for optoelectronically active alkylated-π FMLs has been proposed which will greatly smooth the application of FMLs in various flexible and stretchable electronics.

As featured in:

See Takashi Nakanishi *et al.*,
Chem. Sci., 2018, **9**, 6774.

ROYAL SOCIETY
OF CHEMISTRY

rsc.li/chemical-science

Supercooling of functional alkyl-π molecular liquids†

Fengniu Lu, [ID] [a] Keumhee Jang,[a] Izabela Osica,[b] Keita Hagiwara,[c] Michito Yoshizawa, [ID] [c] Masashi Ishii,[d] Yoshiaki Chino,[e] Kazuchika Ohta, [ID] [e] Kinga Ludwichowska,[b] Krzysztof Jan Kurzydłowski,[b] Shinsuke Ishihara [ID] [a] and Takashi Nakanishi [ID] *[a]

Metastable states of soft matters are extensively used in designing stimuli-responsive materials. However, the non-steady properties may obstruct consistent performance. Here we report an approach to eradicate the indistinguishable metastable supercooled state of functional molecular liquids (FMLs), which remains as a liquid for weeks or months before crystallizing, *via* rational molecular design. The phases (solid, kinetically stable liquid, and supercooled liquid) of a model FML, branched alkyl chain-substituted 9,10-diphenylanthracene (**DPA**), are found to be governed by subtle alterations of the molecular structure (alkyl-**DPA** ratio and bulkiness of the **DPA** unit). We thus outline molecular design principles to avoid supercooled FML formation. Moreover, we demonstrate a practical technique to rapidly discriminate supercooled FMLs (within 5 h) by accelerating their crystallization in differential scanning calorimetry heating *via* pre-annealing or relatively slow scanning.

Introduction

The skillful manipulation of metastable states in stimuli-responsive materials is extensively used for sensing, energy harvesting, biomedical engineering, *etc.*[1] However, materials in metastable states would be destructive for applications requiring consistent performance under various conditions. Considering the metastable matter of supercooled liquids (SCLs) as an example, the kinetically trapped melts below their melting points often crystallize as energetically favoured solids.[2] Such a phase transition in π-conjugated molecular systems always changes the optoelectronic properties.[3] Therefore, SCLs obstruct long-term reliability when used as contributing components in optoelectronic devices. Despite decades of active study, the controllability of SCLs remains challenging because

of their rich phenomenology and complicated phase transition behaviour.[4]

Recently, room-temperature functional molecular liquids (FMLs),[5] which are fluidic and optoelectronically active in nature, have been widely applied in luminescent inks,[6] host–guest binding media,[7] and flexible optoelectronic devices including organic light-emitting diodes,[8] photovoltaics,[9] and organic semiconductors.[10] FMLs are generally prepared by wrapping a π-conjugated molecular unit with bulky and flexible side chains (alkyl,[6,8,11] siloxane,[10b,12] alkylsilyl,[10a,13] or ethylene glycol[7,9a,14]), which suppress the intermolecular π–π interactions and reduce the melting point to below room temperature (20 ± 5 °C). To date, several strategies have been proposed for powerful liquefaction of solid π-molecules.[15] However, some FMLs are SCLs with melting points above room temperature; even when obtained as fluids, they solidify over time.[16] The latent crystallization of supercooled FMLs, which occurs over very long time periods because of the highly amorphous side chains, impedes the identification of SCLs. To guarantee reliable functioning of FMLs-based devices, techniques to disclose indistinguishable supercooled FMLs and molecular design strategies to produce kinetically stable FMLs are necessary.

In this study, we focus on the effects of side chain-content ratio and π-skeleton structure on the phase behaviours of FMLs, aiming to establish molecular design principles for FMLs with kinetic stability at room temperature. As a proof of concept, we report the liquefaction of a model π-conjugated molecule, namely, 9,10-diphenylanthracene (**DPA**) (melting point: 249–250 °C),[17] with bulky and flexible branched alkyl

[a]International Center for Materials Nanoarchitectonics (WPI-MANA), National Institute for Materials Science (NIMS), 1-1 Namiki, Tsukuba 305-0044, Japan. E-mail: nakanishi.takashi@nims.go.jp

[b]Materials Design Division, Faculty of Materials Science and Engineering, Warsaw University of Technology, Woloska 141, 02-507 Warsaw, Poland

[c]Laboratory for Chemistry and Life Science, Institute of Innovative Research, Tokyo Institute of Technology, 4259 Nagatsuta, Midori-ku, Yokohama 226-8503, Japan

[d]Materials Data Platform Center, Research and Services Division of Materials Data and Integrated System (MaDIS), NIMS, 1-2-1 Sengen, Tsukuba 305-0047, Japan

[e]Smart Material Science and Technology, Interdisciplinary Graduate School of Science and Technology, Shinshu University, 1-15-1 Tokida, Ueda 386-8567, Japan

Fig. 1 (a) Chemical structures of DPAn (n = 2, 4, 6, 8, and 10) and DPA8Br. (b) Photographs of freshly synthesized DPAn and DPA8Br in daylight at 20 °C, with a drop of fluid or powder of solid on a glass plate. (c) Photographs of DPA6, DPA8, and DPA10 as fresh (left) and after long-term of aging at ambient temperature (right) taken under irradiation of a UV lamp (365 nm).
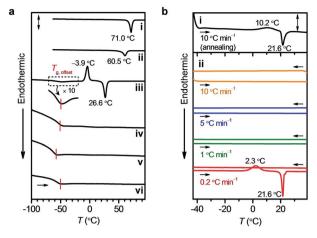

Fig. 2 (a) DSC thermograms of (i) DPA2, (ii) DPA4, (iii) DPA10, (iv) DPA6, (v) DPA8, and (vi) DPA8Br during the first heating scan from −100 to 95 °C at 10 °C min⁻¹ under N₂ flow ($T_{g,offset}$, the offset temperature of the glass-to-isotropic liquid transition; scale bar (sb), 2.0 W g⁻¹ for (i–iii) and 0.2 W g⁻¹ for (iv–vi)). (b) DSC thermograms of DPA8 (i) during the heating scan from −45 to 40 °C at 10 °C min⁻¹ after annealing at −45 °C for 12 h (sb, 0.1 W g⁻¹) and (ii) during the heating/cooling cycles between −45 and 40 °C at 10 °C min⁻¹ (orange; sb, 1.6 W g⁻¹), 5 °C min⁻¹ (blue; sb, 1.6 W g⁻¹), 1 °C min⁻¹ (green; sb, 0.4 W g⁻¹), and 0.2 °C min⁻¹ (red; sb, 0.1 W g⁻¹) under N₂ flow.

chains. Guerbet alcohol-based[18] branched alkyl chains of different lengths were attached to the 3,5-substituent positions of the phenyl units in **DPA** (Fig. 1a, **DPAn**, $n = 2, 4, 6, 8$, and 10, where n denotes the number of carbons in the branched hydrocarbon chain substituted at the β-position of the longer hydrocarbon chain). The compounds with $n \geq 6$ were successfully liquefied (Fig. 1b). However, the kinetic stability of the resulting liquids depended strongly on the alkyl-**DPA** content ratio in the molecular system. Furthermore, by introducing bulky bromine atoms on the 2,6-positions of the anthracene unit, the kinetic stability was efficiently improved (Fig. 1a and b, **DPA8Br**).

Results and discussion

Synthesis of DPA derivatives

DPAn compounds were synthesized via the Williamson ether reaction from 9,10-bis(3,5-dihydroxyphenyl)anthracene and alkyl bromides with yields over 49% (see details in ESI†). The 2,6-dibrominated anthracene **DPA8Br** was prepared via the bromination of 9,10-bis(3,5-dimethoxyphenyl)anthracene, followed by O-demethylation and O-alkylation with 2-octyldodecyl chains. All compounds were unambiguously characterized by ¹H nuclear magnetic resonance (¹H NMR), ¹³C NMR, and matrix-assisted laser desorption ionization-time-of-flight mass spectrometry (MALDI-TOF MS). The ¹H and ¹³C NMR spectra confirmed the absence of residual solvents in all fluidic samples.

Crystallization of supercooled DPA8 and DPA10 promoted by thermal treatment

DPA8, previously reported as a room temperature liquid,[5b] unexpectedly solidified after aging at ambient conditions for over 6 months (Fig. 1c). **DPA10** solidified within 4 weeks from its liquid form (Fig. 1c). To analyze the phase behaviours, we measured thermogravimetric analysis (TGA) and differential scanning calorimetry (DSC) for **DPAn**. TGA confirmed no degradation of any compound below 393 °C (Fig. S1 and Table S1, ESI†). In the DSC heating traces at 10 °C min⁻¹, **DPA2** and **DPA4** exhibit endothermic melting peaks (T_m) at 71.0 °C and 60.5 °C, respectively, whereas **DPA10** exhibits a broad glass-to-

isotropic liquid transition (T_g) (<−50 °C), followed by an exothermic crystallization peak (T_c) at −3.9 °C and a T_m at 26.6 °C (Fig. 2a). According to the thermal behaviours of typical organic crystals summarized in Fig. S2 (ESI†), the fluidic sample of **DPA10** was in a supercooled state below 26.6 °C (Fig. S2c, ESI†). For **DPA6** and **DPA8**, no melting peaks, other than T_g (<−50 °C), are observed in their DSC heating traces (Fig. 2a). However, after annealing at −45 °C for 12 h, subsequent heating induces the crystallization of **DPA8** at 10.2 °C, which thereafter melts at 21.6 °C (Fig. 2b(i)). Therefore, the fluidic sample of **DPA8** at temperatures below 21.6 °C is also in its supercooled state, which crystallizes under cold conditions (Fig. 2b). This result contradicts the previous report that **DPA8** at ambient temperature exists only in liquid form;[5b] thus, FMLs require careful attention to avoid the misuse of their SCL phase.

The effect of annealing on the phase behaviour of **DPA8** can be explained by the crystallization mechanism. The crystallization of an SCL occurs via two steps of nucleation and subsequent crystal growth.[19] Nucleation can occur at any temperature below T_m, but the tendency increases as the temperature decreases between T_m and T_g. Therefore, annealing the **DPA8** SCL at −45 °C, which is just above T_g, promotes nucleation. The generated nuclei grow spontaneously at an elevated temperature (T_c), at which the mobility is sufficient for molecular reorientation and self-organization. Since no T_c was observed in the second heating trace without annealing (Fig. S3, ESI†), we assumed that the time scale of the heating process at 10 °C min⁻¹ was insufficient for **DPA8** crystallization (Fig. S2e, ESI†). Our assumption was approved by the appearance of a crystallization peak at a long heating process with the scan rate reduced to 0.2 °C min⁻¹ (Fig. 2b(ii)). In sharp contrast, the

crystallization of **DPA10** occurred even at 40 °C min^{-1} without annealing (Fig. S4, ESI†). Therefore, **DPA10** exhibits a greater crystallization tendency than **DPA8** does.

DPA6 showed no crystallization peak in the DSC traces even after annealing at −45 °C for 12 h or heating at 0.2 °C min^{-1} (Fig. S5, ESI†). In addition, no solidification was observed during storage at ambient temperature throughout our experimental period (exceeding 1 year) (Fig. 1c). Thus, we conclude that **DPA6** is a kinetically stable liquid at ambient temperatures.[20]

Crystallization tendency governed by alkyl-π ratio and the bulkiness of the π-unit

Judging from the phase behaviours of **DPA2** → **DPA6**, lengthening the alkyl chains reduces the melting point. According to the decreased entropy values from **DPA4** (111.0 J mol^{-1} K^{-1}) to **DPA2** (131.8 J mol^{-1} K^{-1}) at their respective melting temperatures (Table S1, ESI†), solid **DPA4** has a larger amorphous content than solid **DPA2**. For **DPA6**, the amorphousness may be further enhanced by its bulkier and more random alkyl side chains, thus suppressing solidification.

On the other hand, from **DPA6** → **DPA10**, lengthening the alkyl chains enhances the crystallization tendency of the melts. To gain deeper insight, the distribution of **DPA** units in **DPA6**, **DPA8**, and **DPA10** melts at 30 °C was investigated. All three melts were isotropic liquids, as confirmed by the absence of birefringence in polarized optical microscopic (POM) observations (Fig. S6, ESI†). Their liquid-like behaviours were suggested by the higher values for viscous loss moduli (G'') than for storage elastic moduli (G') throughout the measured angular frequency (ω) range (Fig. S7, ESI†). The subsequent small- and wide-angle X-ray scattering (SWAXS) measurements verified the lack of long-range molecular ordering, as no sharp crystalline peaks were detected (Fig. 3a). The average intermolecular **DPA**–**DPA** distances (taken from the top of the halo appearing in the small-angle region) in **DPA6** (18.9 Å), **DPA8** (21.0 Å), and **DPA10** (22.0 Å) were much larger than that for active π–π interactions (3.4–3.5 Å), indicating negligible interactions among adjacent **DPA** units. We thus hypothesize that the increased crystallization tendency from **DPA6** → **DPA10** might originate from increased van der Waals interactions among alkyl chains of longer lengths.[3b] In addition, when the length of alkyl chains increases from **DPA6** → **DPA10**, the low-q halo become narrower (Fig. 3a, full width at half maximum was calculated as
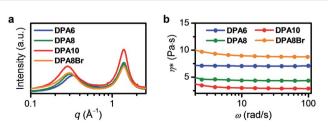
0.26 Å^{-1} for **DPA6**, 0.22 Å^{-1} for **DPA8**, and 0.19 Å^{-1} for **DPA10**), suggesting improved regularity of intermolecular distances. Such an improvement is probably caused by the more uniform molecular shape, e.g., more globular-like, with longer alkyl side chains, which may also contribute to the enhanced crystallization tendency.

The viscosity of liquid is also influenced by the alkyl-**DPA** ratio. As confirmed by the order of complex viscosity (η^*) of the melts at 30 °C (at angular frequency (ω) = 10 rad s^{-1}) of **DPA10** (3.0 Pa s) < **DPA8** (4.4 Pa s) < **DPA6** (7.1 Pa s) (Fig. 3b and Table S1, ESI†), higher alkyl chain contents promote greater molecular softening and thus increase fluidity. Consequently, **DPA10** and **DPA8** may experience faster molecular diffusion, which can facilitate crystallization. Therefore, it can be concluded that the kinetic stability of alkylated-π FMLs is governed by the alkyl-π ratio.

In addition, we introduced bromine atoms on the 2,6-positions of anthracene in **DPA8**, yielding the kinetically stable liquid of **DPA8Br** (Fig. 1a and b). No crystallization is observed either in the DSC measurements (Fig. 2a and S8, ESI†) or after long-term (>1 year) aging at ambient temperature. Possible reasons for the suppressed crystallization of **DPA8Br** include a decrease of π-skeleton symmetry from D_{2h} to C_{2h} and a higher η^* (9.0 Pa s) than that of **DPA8** (4.4 Pa s) (Fig. 3b and Table S1, ESI†). The increased viscosity may originate from the larger molecular size of **DPA8Br**. As supported by SWAXS analysis, the average core-to-core distance of **DPA8Br** (21.3 Å) is slightly larger than that of **DPA8** (21.0 Å) (Fig. 3a).

Structural and photophysical changes of DPA8 and DPA10 upon SCL-to-crystal transition

To identify the molecular organization during crystallization, variable-temperature SWAXS and POM studies were performed
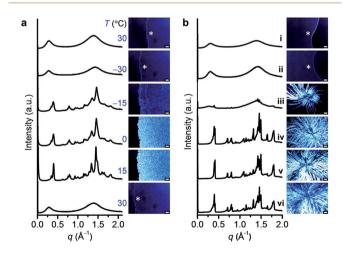

Fig. 4 (a) Variable-temperature SWAXS profiles (left) and POM images (right; scale bar (sb), 50 μm) of **DPA10** cooled from 30 to −30 °C, and then heated to −15, 0, 15, and 30 °C at 10 °C min^{-1} (top to down). (b) SWAXS profiles (left) and POM images (right; sb, 50 μm for (i–iii) and 100 μm for (iv–vi)) of **DPA8**: (i) freshly melted, (ii) annealed at −18 °C for 1 day, and subsequent aging at 15 °C for (iii) 1 day, (iv) 3 days, (v) 7 days, and (vi) 14 days. The sample area was denoted with asterisk (*) in the POM.

Fig. 3 (a) SWAXS profiles and (b) complex viscosity (η^*) of **DPA6** (blue), **DPA8** (green), **DPA10** (red), and **DPA8Br** (orange) at 30 °C (ω, angular frequency).

for **DPA10**; the results agreed well with the DSC findings. As **DPA10** was cooled from 30 to −30 °C, the broad halos in the SWAXS profile and the dark sample region in the POM image (Fig. 4a) were retained, indicating supercooling of the melt. Upon heating from −30 to −15 °C at 10 °C min⁻¹, crystalline peaks were detected by SWAXS and birefringence was observed *via* POM in the SCL domain. The peaks in the SWAXS profiles sharpened and intensified, and the texture in the POM images gradually propagated throughout the sample area as the temperature was elevated from −15 to 15 °C. Further heating to 30 °C caused the collapse of all SWAXS sharp peaks and POM texture (see also Movie S1, ESI†) due to the melting of the crystalline phase. The profile at 15 °C exhibited multiple peaks (Fig. 4a). However, all peaks were relatively broad. Moreover, the broad halo at the wide-angle region (4.5 Å), which corresponds to the mean distance between molten alkyl chains (Fig. 3a), remained in the profile. Thus, the crystalline sample of **DPA10** is partially amorphous, resembling a liquid crystalline phase. However, pressing and shear caused no changes in the POM texture (Fig. S10, ESI†). And the enthalpy values at T_c and T_m of the DSC curve are quite high (Table S1, ESI†). Therefore, **DPA10** is not only partially amorphous but also partially crystalline.

The crystallization of **DPA8** was also monitored *via* SWAXS and POM (Fig. 4b), by annealing the sample at −18 °C [21] for 1 day and then holding it at 15 °C. Multiple peaks in the SWAXS profile and birefringence texture on the POM image appeared after aging at 15 °C for 1 day. After 7 days, crystallization ceased. POM images show a dendritic texture (Fig. 4b) with a larger domain size than the spherulite texture of **DPA10** formed *via* a slow crystallization process by annealing the melted sample at −5 °C for 7 h (Fig. S9a, ESI†). As further reflected in the SWAXS profiles, crystalline **DPA8** exhibited a larger number of sharp peaks and a less intense alkyl halo (Fig. 4b) than did **DPA10** (Fig. S9b, ESI†). The molecular packing structures in the crystalline states of both **DPA8** and **DPA10** were difficult to determine because of their complex patterns, which showed larger numbers of peaks than those of any considerable liquid crystals, and both broader and fewer peaks than those of the presumed single-crystalline materials.

To analyze the influence of the SCL-to-crystal transition on the optical characteristics, the photophysical properties of **DPA***n* were studied. The melts of **DPA6**, **DPA8**, and **DPA10** showed optical features comparable to those of their dilute solutions (Fig. S11 and Table S2, ESI†), confirming the absence of significant intermolecular interactions among the solvent-free **DPA** chromophores. Fig. 5a shows good spectral consistence between liquid **DPA6** and SCLs of **DPA8** and **DPA10**, further indicating that the supercooled state is indistinguishable by spectroscopic features. The more vibronic structure of the fluorescence bands of **DPA8** and **DPA10** may originate from their lower viscosities. Upon crystallization, the emission bands of **DPA8** and **DPA10** become less vibronic (with the disappearance of the 411 nm shoulder peak) and slightly blue-shifted (Fig. 5a). The spectral shift is ascribed to increased molecular organization, rather than restricted molecular motion, in the solid crystalline state. As confirmed by the temperature-variable fluorescence spectra of **DPA10**, negligible spectral shift is
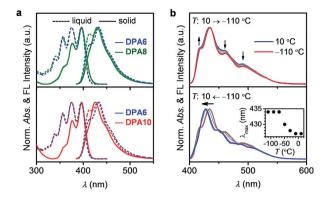

Fig. 5 (a) Normalized UV-vis absorption (left) and fluorescence (right) spectra of **DPA6** (blue), **DPA8** (green) and **DPA10** (red) as liquid (dashed line) and crystalline (solid line) at 20 °C. (b) Variable-temperature fluorescence spectra of **DPA10** measured at 20 °C steps during cooling from 10 to −110 °C (up) and subsequent heating from −110 to 10 °C (below; inset, maximum emission wavelength at each temperature) at 10 °C min⁻¹.

observed when the sample is frozen into the amorphous glass state upon cooling from 10 to −110 °C (Fig. 5b, up). However, subsequent heating to above −50 °C (at which crystallization could occur) causes a hypsochromic shift of the emission band (Fig. 5b, below). According to these results, the crystallization of a luminescent supercooled FML leads to non-steady photophysical properties.

Conclusions

We elucidate the issue of supercooling of FMLs for the first time and propose effective measures to distinguish and eradicate the undesired metastable matter. By liquefying a solid π-molecule, 9,10-diphenylanthracene, with branched alkyl chains and further modifying the anthracene core with bulky atoms, we clarify three fundamental factors to prohibit the formation of supercooled FMLs: (i) a delicate alkyl chain-to-π ratio, (ii) a bulkier π-unit, and (iii) a less symmetric π-skeleton. These findings are essential to avoid the misuse of SCLs with non-steady functions and facilitate long-term practical applications of FMLs. In addition, rapid discrimination of supercooled FMLs is enabled by appropriate thermal treatment that accelerates the crystallization process. Deeper studies of the effect of π-skeleton structure on the kinetic stability of FMLs and the organization of supercooled molecules during crystallization would aid the development of advanced molecular design methodologies for the production of more reliable functional soft materials. Research in this direction is in progress.

Conflicts of interest

There are no conflicts to declare.

Acknowledgements

Notes and references

1 (a) H. Wang, H. K. Bisoyi, L. Wang, A. M. Urbas, T. J. Bunning and Q. Li, *Angew. Chem., Int. Ed.*, 2018, **57**, 1627–1631; (b) K. G. Gutierrez-Cuevas, L. Wang, Z. Zheng, H. K. Bisoyi, G. Li, L.-S. Tan, R. A. Vaia and Q. Li, *Angew. Chem., Int. Ed.*, 2016, **55**, 13090–13094; (c) S. Yagai, S. Okamura, Y. Nakano, M. Yamauchi, K. Kishikawa, T. Karatsu, A. Kitamura, A. Ueno, D. Kuzuhara, H. Yamada, T. Seki and H. Ito, *Nat. Commun.*, 2014, **5**, 4013.

2 (a) P. G. Debenedetti and F. H. Stillinger, *Nature*, 2001, **410**, 259–267; (b) M. D. Ediger, C. A. Angell and S. R. Nagel, *J. Phys. Chem.*, 1996, **100**, 13200–13212.

3 (a) S. Karasawa, R. Hagihara, Y. Abe, N. Harada, J.-i. Todo and N. Koga, *Cryst. Growth Des.*, 2014, **14**, 2468–2478; (b) K. Chung, M. S. Kwon, B. M. Leung, A. G. Wong-Foy, M. S. Kim, J. Kim, S. Takayama, J. Gierschner, A. J. Matzger and J. Kim, *ACS Cent. Sci.*, 2015, **1**, 94–102; (c) Y. Sagara, K. Kubo, T. Nakamura, N. Tamaowki and C. Weder, *Chem. Mater.*, 2017, **29**, 1273–1278; (d) K. Mase, Y. Sasaki, Y. Sagara, N. Tamaoki, C. Weder, N. Yanai and N. Kimizuka, *Angew. Chem., Int. Ed.*, 2018, **57**, 2806–2810.

4 (a) K. Paeng and L. J. Kaufman, *Chem. Soc. Rev.*, 2014, **43**, 977–989; (b) E. Brini, C. J. Fennell, M. Fernandez-Serra, B. Hribar-Lee, M. Lukšič and K. A. Dill, *Chem. Rev.*, 2017, **117**, 12385–12414.

5 (a) T. Michinobu, T. Nakanishi, J. P. Hill, M. Funahashi and K. Ariga, *J. Am. Chem. Soc.*, 2006, **128**, 10384–10385; (b) P. Duan, N. Yanai and N. Kimizuka, *J. Am. Chem. Soc.*, 2013, **135**, 19056–19059; (c) M. J. Hollamby, M. Karny, P. H. H. Bomans, N. A. J. M. Sommerdjik, A. Saeki, S. Seki, H. Minamikawa, I. Grillo, B. R. Pauw, P. Brown, J. Eastoe, H. Möhwald and T. Nakanishi, *Nat. Chem.*, 2014, **6**, 690–696; (d) N. Giri, M. G. Del Pópolo, G. Melaugh, R. L. Greenaway, K. Rätzke, T. Koschine, L. Pison, M. F. C. Gomes, A. I. Cooper and S. L. James, *Nature*, 2015, **527**, 216–220.

6 (a) S. S. Babu, J. Aimi, H. Ozawa, N. Shirahata, A. Saeki, S. Seki, A. Ajayaghosh, H. Möhwald and T. Nakanishi, *Angew. Chem., Int. Ed.*, 2012, **51**, 3391–3395; (b) S. S. Babu, M. J. Hollamby, J. Aimi, H. Ozawa, A. Saeki, S. Seki, K. Kobayashi, K. Hagiwara, M. Yoshizawa, H. Möhwald and T. Nakanishi, *Nat. Commun.*, 2013, **4**, 1969.

7 (a) T. Ogoshi, T. Aoki, R. Shiga, R. Iizuka, S. Ueda, K. Demachi, D. Yamafuji, H. Kayama and T.-a. Yamagishi, *J. Am. Chem. Soc.*, 2012, **134**, 20322–20325; (b) J. Zhang, S.-H. Chai, Z.-A. Qiao, S. M. Mahurin, J. Chen, Y. Fang, S. Wan, K. Nelson, P. Zhang and S. Dai, *Angew. Chem., Int. Ed.*, 2015, **54**, 932–936.

8 (a) S. Hirata, K. Kubota, H. H. Jung, O. Hirata, K. Goushi, M. Yahiro and C. Adachi, *Adv. Mater.*, 2011, **23**, 889–893;

(b) N. Kobayashi, T. Kasahara, T. Edura, J. Oshima, R. Ishimatsu, M. Tsuwaki, T. Imato, S. Shoji and J. Mizuno, *Sci. Rep.*, 2015, **5**, 14822.

9 (a) H. J. Snaith, S. M. Zakeeruddin, Q. Wang, P. Péchy and M. Grätzel, *Nano Lett.*, 2006, **6**, 2000–2003; (b) T. J. Kramer, S. S. Babu, A. Saeki, S. Seki, J. Aimi and T. Nakanishi, *J. Mater. Chem.*, 2012, **22**, 22370–22373.

10 (a) B. A. Kamino, T. P. Bender and R. A. Klenkler, *J. Phys. Chem. Lett.*, 2012, **3**, 1002–1006; (b) T. G. Plint, B. A. Kamino and T. P. Bender, *J. Phys. Chem. C*, 2015, **119**, 1676–1682.

11 (a) S. S. Babu and T. Nakanishi, *Chem. Commun.*, 2013, **49**, 9373–9382; (b) A. Ghosh and T. Nakanishi, *Chem. Commun.*, 2017, **53**, 10344–10357; (c) K. Masutani, M. Morikawa and N. Kimizuka, *Chem. Commun.*, 2014, **50**, 15803–15806; (d) M. J. Hollamby, A. E. Danks, Z. Schnepp, S. E. Rogers, S. R. Hart and T. Nakanishi, *Chem. Commun.*, 2016, **52**, 7344–7347; (e) F. Lu, T. Takaya, K. Iwata, I. Kawamura, A. Saeki, M. Ishii, K. Nagura and T. Nakanishi, *Sci. Rep.*, 2017, **7**, 3416; (f) Z. Agnieszka, T. Atsuro, S. Hiroya, S. Akinori, L. Marcin and N. Takashi, *Chem.–Asian J.*, 2018, **13**, 770–774; (g) B. Narayan, K. Nagura, T. Takaya, K. Iwata, A. Shinohara, H. Shinmori, H. Wang, Q. Li, X. Sun, H. Li, S. Ishihara and T. Nakanishi, *Phys. Chem. Chem. Phys.*, 2018, **20**, 2970–2975.

12 (a) B. A. Kamino, J. B. Grande, M. A. Brook and T. P. Bender, *Org. Lett.*, 2010, **13**, 154–157; (b) E. M. Maya, A. W. Snow, J. S. Shirk, R. G. S. Pong, S. R. Flom and G. L. Roberts, *J. Mater. Chem.*, 2003, **13**, 1603–1613.

13 M. Taki, S. Azeyanagi, K. Hayashi and S. Yamaguchi, *J. Mater. Chem. C*, 2017, **5**, 2142–2148.

14 C.-H. Shim, S. Hirata, J. Oshima, T. Edura, R. Hattori and C. Adachi, *Appl. Phys. Lett.*, 2012, **101**, 113302.

15 (a) M. J. Hollamby and T. Nakanishi, *J. Mater. Chem. C*, 2013, **1**, 6178–6183; (b) F. Lu and T. Nakanishi, *Sci. Technol. Adv. Mater.*, 2015, **16**, 014805.

16 (a) T. Machida, R. Taniguchi, T. Oura, K. Sada and K. Kokado, *Chem. Commun.*, 2017, **53**, 2378–2381; (b) L. C. Kerkhof, K. M. Allan, K. M. McGrath, J. L. Spencer and J. M. Hodgkiss, *Int. J. Nanotechnol.*, 2017, **14**, 432.

17 C. K. Ingold and P. G. Marshall, *J. Chem. Soc.*, 1926, **129**, 3080–3089.

18 A. J. O'Lenick, *J. Surfactants Deterg.*, 2001, **4**, 311–315.

19 F. Abraham, *Homogeneous Nucleation Theory*, Academic Press, New York, 1974.

20 For accuracy, "kinetically stable" was used in this manuscript, because it is difficult to prove that **DPA6** is "thermodynamically stable". Even under more strict conditions (annealing at -45 °C for 24 h or applying slow scan rate of 0.2 °C min^{-1} after annealing at -45 °C for 12 h), no crystallization peak was observed in the DSC heating trace.

21 The lowest temperature we can regulate to stock the samples for SWAXS measurements and POM observation.